CRYSTAL GROWTH & DESIGN
2005
VOL. 5, NO. 4
1527−1530

Y_2O_3 Microprisms with Trilobal Cross Section

Jie Zhang,[†] Zhiguo Liu,[‡] Jun Lin,*[,†] and Jiye Fang[§]

Key Laboratory of Rare Earth Chemistry and Physics and State Key Laboratory of Electroanalytical Chemistry, Changchun Institute of Applied Chemistry, Chinese Academy of Sciences, 5625 Renmin Street, Changchun 130022, China, and Department of Chemistry and Advanced Materials Research Institute, University of New Orleans, New Orleans, Louisiana 70148

Received October 25, 2004; Revised Manuscript Received March 3, 2005

ABSTRACT: Yttrium oxide (Y_2O_3) microprisms with interesting trilobal cross section were synthesized through a large-scale and facile hydrothermal method followed by a subsequent heat treatment. The size of the Y_2O_3 trilobal prisms could be modulated from micro- to submicroscale with the increase of pH value. The as-formed products via the hydrothermal process, monoclinic yttrium oxide hydroxide nitrate, $Y_4O(OH)_9(NO_3)$, could transform to cubic Y_2O_3 with the same morphology after annealing at high temperatures. The formation mechanism for the $Y_4O(OH)_9(NO_3)$ trilobal prisms has been proposed. Under hydrothermal conditions, the synergistic effect of Y-type aggregates of primary $Y_4O(OH)_9(NO_3)$ nanorods and sequent preferential of different crystal planes resulted in the formation of trilobal prisms.

1. Introduction

One-dimensional (1D) nanostructures, including nanorods, nanowires, nanotubes, and nanoprisms have attracted extensive synthetic interests over the past several years due to their potential applications in a wide range of fields.[1−5] More applications and new functional materials might emerge if shape-controlled nanocrystals could be achieved with high complexity.[6,7] Yttrium oxide (Y_2O_3) is an important engineering material in many fields such as optics, optoelectronics, advanced ceramics, and insulators, as well as high-efficiency additives for composite materials of high performance.[8−10]

The unique structure, geometric shape, and specific properties of trilobal fibers have had a high impact on applications in the textile industry. Trilobal synthetic or chemical fibers made from many starting materials are used extensively to manufacture a number of fabrics with ameliorated properties compared with those of fabrics from round fibers. The fiber profile plays an important role in determining the mechanical and surface properties of fabrics.[11−14] For example, G. K. Tyagi[11] reported that that both ring and rotor yams spun with trilobal polyester fibers have lower tenacity, higher breaking extension, more twist liveliness, lower work of rupture, and higher flexural rigidity. Furthermore, lower yam-to-metal friction, higher dye pick-up, and low hairiness can be obtained for blended yams having polyester fibers of noncircular cross section. However, to our knowledge, among trilobal inorganic materials, only trilobal SiC and carbon fiber were reported, which also were produced by sequent heat treatment of the as-formed trilobal precursor fibers through spinnerets with trilobal holes, which is the general technology and equipment in the textile industry to make trilobal fibers.[15,16] In this contribution, we demonstrate our first synthesis of Y_2O_3 microprisms with trilobal cross section through a large-scale and facile hydrothermal process followed by subsequent heat treatment.

2. Experimental Section

In a typical synthesis, 1 mmol of commercial Y_2O_3 (99.99%) was dissolved into 10 mL of diluted nitric acid (20 wt %) under heating to form a solution. After evaporation, 35 mL of deionized water was added to form a clear aqueous solution. Then 25 wt % of ammonia solution (A.R.) was introduced dropwise to the vigorously stirred solution until pH = 8−11. After additional agitation for 15 min, the as-obtained colloidal precipitate was transferred to a 50 mL autoclave, sealed, and heated at 200 °C for 24 h. The autoclave was then cooled to room-temperature naturally. The precursors were recovered by filtration, washing with deionized water for three times, and drying at 60 °C in air for 4 h. The final products were retrieved through a heat treatment at 1000 °C in air.

The samples were characterized by powder X-ray diffraction (XRD) on a Rigaku-Dmax 2500 diffractometer with Cu Kα radiation (λ = 0.154 05 nm) and field emission scanning electron microscopy (FE-SEM, XL30, Philips). TGA-DSC data were recorded with Thermal Analysis Instrument (SDT 2960, TA Instruments, New Castle, DE) with the heating rate of 10 °C·min^{-1} in an air flow of 100 mL·min^{-1}.

3. Results and Discussion

The purity and crystallinity of the products were examined using powder X-ray diffraction (XRD). The XRD peaks for the as-formed products through the hydrothermal process (Figure 1) can be indexed to a monoclinic lattice [space group: $P2_1/4$] of pure yttrium oxide hydroxide nitrate, $Y_4O(OH)_9(NO_3)$. The calculated lattice constants, a = 0.933 nm, b = 1.629 nm, c = 0.362 nm, and β = 100.97°, are in good agreement with those values (a = 0.937 nm, b = 1.637 nm, c = 0.362 nm, and β = 101.17°) from the standard card (JCPDS no. 79-1352).

* To whom correspondence should be addressed. E-mail: jlin@ns.ciac.jl.cn. Fax: +86-431-5698041. Tel: +86-431-5262031.
[†] Key Laboratory of Rare Earth Chemistry and Physics, Changchun Institute of Applied Chemistry, Chinese Academy of Sciences.
[‡] State Key Laboratory of Electroanalytical Chemistry, Changchun Institute of Applied Chemistry, Chinese Academy of Sciences.
[§] Department of Chemistry and Advanced Materials Research Institute, University of New Orleans.

10.1021/cg049640u CCC: $30.25
Published on Web 04/09/2005

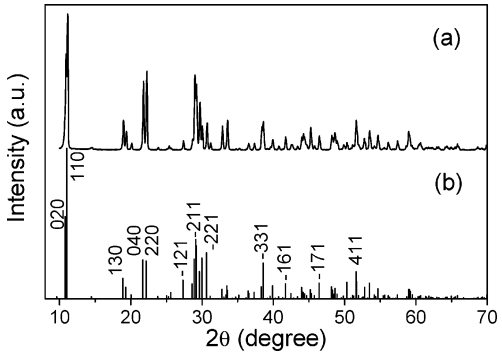

Figure 1. XRD patterns of (a) the as-formed trilobal prisms and (b) the JCPDS card 79-1352 for $Y_4O(OH)_9(NO_3)$.

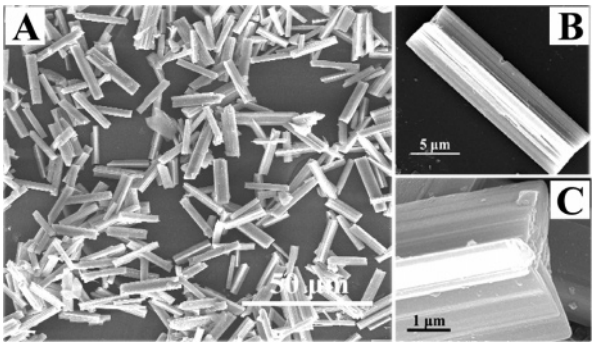

Figure 2. FESEM images of $Y_4O(OH)_9(NO_3)$ trilobal prisms: (A) wide-field; (B) a side view of a single prism; (C) a magnified image of the cross section (pH = 8).

Figure 2A is a wide-field field emission scanning electron microscopy (FESEM) image observed from the as formed precursors (pH = 8), clearly indicating that the samples are entirely comprised of trilobal prisms (about 18 μm in length and aspect ratio about 5). Figure 3A,B gives the histograms of length and aspect ratio distribution of these trilobal prisms. The top-right inset [Figure 2B] presents a magnified view of single prism along the axial direction. The bottom-right inset [Figure 2C] shows the image of a cross section of single prism. These insets confirm that the prisms have shapely trilobal structure. As illustrated in Figure 4, the size of trilobal prisms can be modulated by changing the synthetic conditions. When the pH values of the colloids increased from 8 to 11 with increase in the amount of ammonia solution, for example, the diameter of trilobal prisms decreased from micrometer scale to submicrometer scale, as shown in Figure 2A (pH = 8) and in Figure 4A,C (pH = 10 and 11), respectively. It is also worth mentioning that the mean aspect ratio also increases as the pH value increases. For instance, a synthesis for pH = 8 yielded trilobal prisms with a mean aspect ratio of ~5 [Figure 3B]; whereas a reaction for pH = 10 and 11 resulted in products with a mean aspect ratio of ~7 and ~10 [Figure 4B,D], respectively. This can be attributed to the fact that under high-pH conditions, the nucleating process occurs faster and more nuclei of crystal form, giving a high aspect ratio. The phenomenon is similar to the connection of pH values with the diameters of nanorods in the work of Li[3] and Qian.[17]

The growth process of the trilobal prisms through hydrothermal process was investigated by observing the

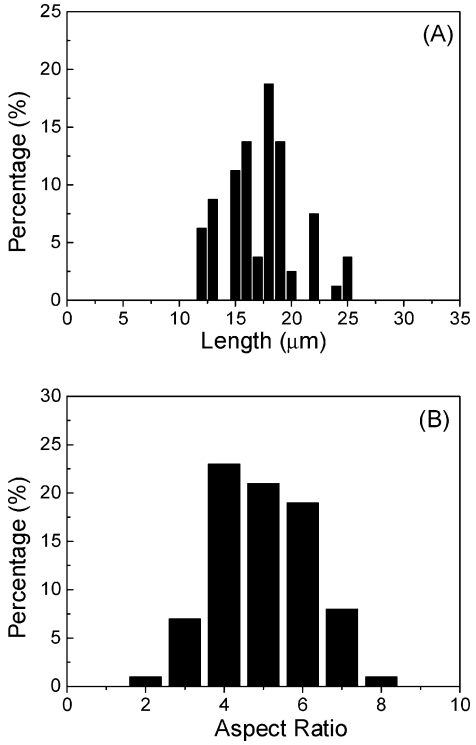

Figure 3. Histogram of (A) length distribution and (B) aspect ratio of $Y_4O(OH)_9(NO_3)$ trilobal prisms.

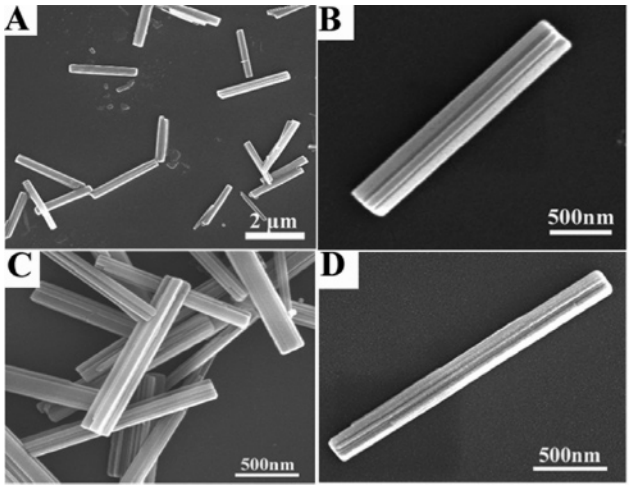

Figure 4. FESEM images of $Y_4O(OH)_9(NO_3)$ trilobal prisms synthesized at (A, B) pH = 10 and (C, D) pH = 11.

images of prisms at different stages, as shown in Figure 5. Verified by XRD study, the initial irregular nanosheets from the hydrothermal solution were determined as a metastable phase, $Y_2(OH)_5(NO_3)\cdot 1.5H_2O$ (see Figure 6). After a phase transformation, the nucleation to form $Y_4O(OH)_9(NO_3)$ would occur, and there was an intrinsic tendency to grow into rodlike nanopartilces due to its anisotropic monoclinic structure, which is similar to the nucleation and anisotropic growth of $La(OH)_3$ under hydrothermal conditions.[3,17] These nanorods, as seeds, rapidly self-assembled into arrays with Y-type structure along their cross-sectional diameter direction through a direct aggregation growth process, which is probably because the crystal facets along the cross-sectional diameter direction match well, offering a low surface energy. Then the crystal planes along the prism axial

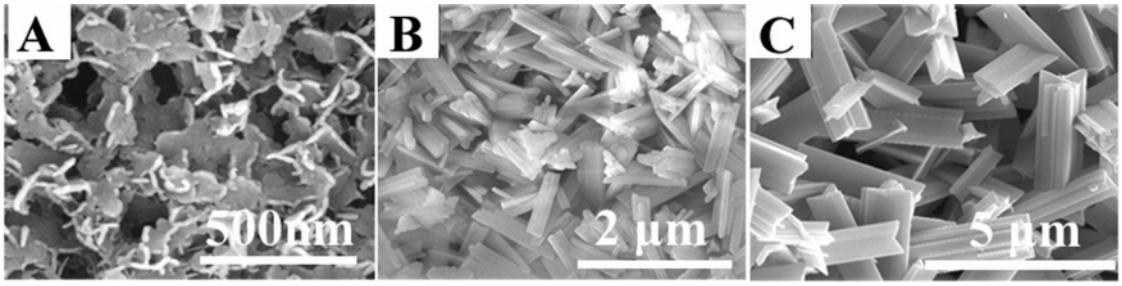

Figure 5. FESEM images of different growth stages: (A) 2 h, $Y_2(OH)_5(NO_3)\cdot 1.5H_2O$ nanosheets; (B) 2.5 and (C) 3.5 h, $Y_4O(OH)_9(NO_3)$ trilobal prisms.

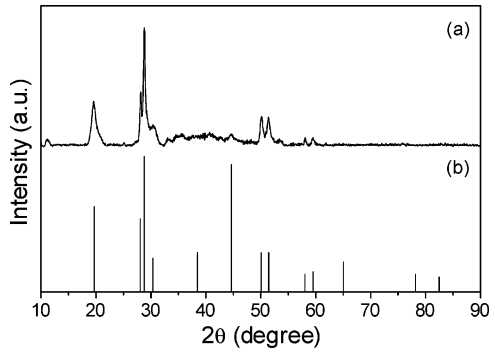

Figure 6. XRD patterns of (a) the sample hydrothermally treated for 2 h and (b) JCPDS no. 49-1107 for $Y_2(OH)_5(NO_3)\cdot 1.5H_2O$.

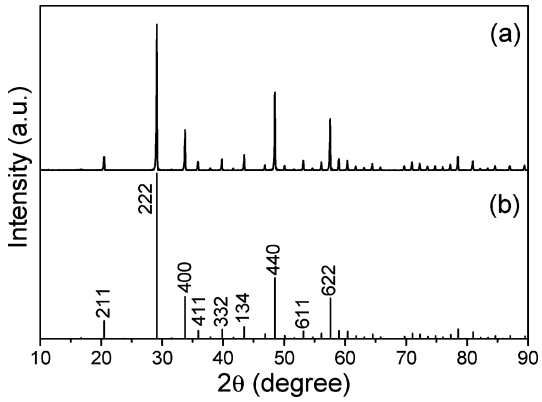

Figure 7. XRD patterns of (a) the trilobal prisms after heat treatment and (b) JCPDS no. 83-0927 for Y_2O_3.

direction and the extension direction of lamina grew preferentially, while the crystal plane perpendicular to the lamina grew relatively slowly. This resulted in formation of the trilobal-type prisms finally. The process is illustrated in Scheme 1. The different growing rates of various crystal planes might associate with their surface energies.

A strong basic NaOH and a weak basic diethylamine were also tried under the same experimental conditions, but for the former, circular microrods were obtained, which coincides with the Y. D. Li's report;[3] whereas irregular laminar crystals were the product for the latter. It is concluded from the above comparison that NH_4^+ does play an important role in the formation of trilobal prisms; however, the exact mechanism requires further systematic and extensive study. Since a high-resolution transmission electron microscopy (HRTEM) image was unable to be collected due to the instability of the $Y_4O(OH)_9(NO_3)$ under the bombardment of the electron beam, the as-mentioned crystal planes are difficult to confirm. This is probably because $Y_4O(OH)_9(NO_3)$ contains many OH^-, which are easy to escape at some forms under high electron beams on a selected area. To our surprise, the phase transformation and growth process could finish merely during half an hour according to the XRD monitoring, indicating that the nucleation and growth of the trilobal prisms proceed very fast. During the continuous growth, these prisms continue to grow up to more uniform prisms and separate from each other [see Figure 5C].

After subsequent heat treatment, the monoclinic $Y_4O(OH)_9(NO_3)$ transform into cubic Y_2O_3, as identified in Figure 7. Figure 8 shows the thermogravimetric analysis (TGA)−differential scanning calorimetry (DSC) curves of $Y_4O(OH)_9(NO_3)$ crystals. It indicates that there are two weight loss stages: 398 and 511 °C, accompanying their corresponding endothermic peaks. The weight loss for the two stages and the total weight loss are 11.29%, 10.13%, and 22.60%, respectively. The measured total weight loss is in agreement with the calculated value: 23.01%. But considering the complex decomposition of $Y_4O(OH)_9(NO_3)$ crystals, we are unable to know the exact decomposition mechanism of $Y_4O(OH)_9(NO_3)$ crystals. At 914.77 °C, there is a small exothermic peak, which suggests the perfection of Y_2O_3 crystallization. However, the trilobal prism structure remained even after a heat treatment at 1000 °C for 2 h. Figure 9

Scheme 1. Schematic Illustration Showing the Formation Mechanism of $Y_4O(OH)_9(NO_3)$ Trilobal Prisms

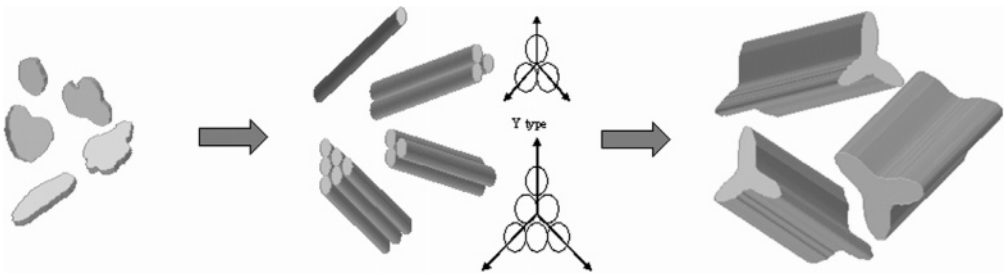

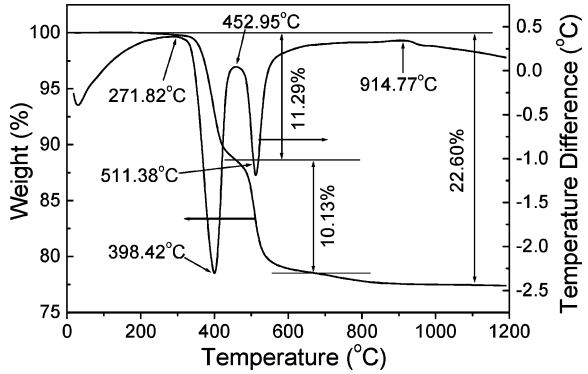

Figure 8. TGA−DSC curves of $Y_4O(OH)_9(NO_3)$ trilobal crystals.

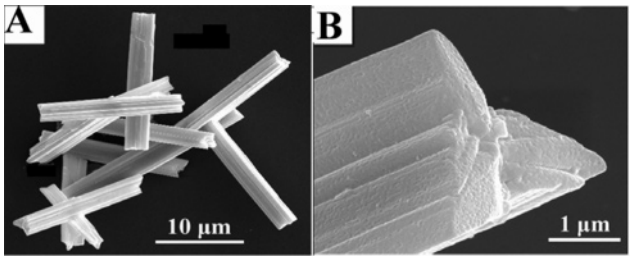

Figure 9. FESEM images of Y_2O_3 trilobal prisms: (A) wide-field; (B) a magnified image of the cross section.

exhibits that the length and diameter of the trilobal prisms are almost as same as those prior to the heat treatment (the sample in Figure 9 used the sample in Figure 1 as a precursor for heat treatment). During the decomposition process, monoclinic $Y_4O(OH)_9(NO_3)$ gradually loses some elements and transforms to cubic Y_2O_3. Although the phase transformation occurs, the formation of cubic phase does not result in the collapse of prisms to particles. Moreover, the phase transformation progresses simultaneously and anisotropically. This does not lead to shrinkage strain of the prisms, or the degree of shrinkage in every direction is almost identical, so the trilobal structure remains. This phenomenon is similar to some other reports. For example, hexagonal $Y(OH)_3$ nanorods and nanotubes can be transformed to cubic Y_2O_3 nanorods and nanotubes under high temperature with the same morphology.[2,3]

4. Conclusion

In summary, Y_2O_3 microprisms with trilobal cross section have been prepared via a facile hydrothermal process followed by a subsequent heat treatment. These materials with special structure may be useful for some specific applications and serve as templates to synthesize other nanostructural and functional materials. Further work including a preparation of other rare earth oxides with similar prism structure and use of these prisms as templates to produce other functional and composite materials is under way.

Acknowledgment. This project is financially supported by the foundation of "Bairen Jihua" of Chinese Academy of Sciences, the MOST of China (No. 2003CB314707), and the National Natural Science Foundation of China (Grants 50225205, 20271048, and 20431030). Prof. Fang is grateful for the financial support by the foundation of a two-base program for international cooperation of NSFC (Grant 00310530) and NSF Grant DMR-0449580.

References

(1) Xia, Y. N.; Yang, P. D.; Sun, Y. G.; Wu, Y. Y.; Mayers, B.; Gates, B.; Yin, Y. D.; Kim, F.; Yan, H. Q. *Adv. Mater.* **2003**, *15*, 353−389.
(2) Wang, X.; Sun, X. M.; Yu, D. P.; Zou, B. S.; Li, Y. D. *Adv. Mater.* **2003**, *15*, 1442−1445.
(3) Wang, X.; Li, Y. D. *Angew. Chem., Int. Ed.* **2002**, *41*, 4790−4793.
(4) Jin, R. C.; Cao, Y. W.; Mirkin, C. A.; Kelly, K. L.; Schatz, G. C.; Zheng, J. *Science* **2001**, *294*, 1901−1903.
(5) Ghezelbash, A.; Sigman, M. B., Jr.; Korgel, B. A. *Nano Lett.* **2004**, *4*, 537−542.
(6) Manna, L.; Milliron, D. J.; Meisel, A.; Scher, E. C.; Alivisatos, A. P. *Nat. Mater.* **2003**, *2*, 382−385.
(7) Hao, E. C.; Bailey, R. C.; Schatz, G. C.; Hupp, J. T.; Li, S. Y. *Nano Lett.* **2004**, *4*, 327−330.
(8) Piticescu, R. M.; Piticescu, R. R.; Taloi, D.; Badilita, V. *Nanotechnology* **2003**, *14*, 312−317.
(9) Ivanic, R.; Breternitz, V.; Tvarozek, V.; Novotny, I.; Knedlik, C.; Rehacek, V. *J. Electr. Eng.* **2003**, *54*, 83−87.
(10) Wen, L.; Sun, X. D.; Xiu, Z. M.; Chen, S. W.; Tsai, C. T. *J. Eur. Ceram. Soc.* **2004**, *24*, 2681−2688.
(11) Tvagi, G. K.; Sharma, K. R.; Goval, A.; Singh, M. *Indian J. Fibre Text. Res.* **2004**, *29*, 184−189.
(12) Alston, P. V.; Hansen, S. M.; Duncan, P. J. *Text. Res. J.* **2002**, *72*, 352−356.
(13) Fouda, I. M.; Shabana, H. M. *Eur. Polym. J.* **2000**, *36*, 823−829.
(14) Kim, C.; Cho, G.; Hong, K. A.; Shim. H. J. *Fibers Polym.* **2003**, *4*, 199−203.
(15) Wang, Y. D.; Chen, Y. M.; Zhu, M. F. *J. Mater. Sci. Lett.* **2002**, *21*, 349−350.
(16) Lee, Y. S.; Basova, Y. V.; Edie, D. D.; Reid, L. K.; Newcombe, S. R.; Ryu, S. K. *Carbon* **2003**, *41*, 2573−2584.
(17) Tang, Q.; Liu, Z. P.; Li, S.; Zhang, S. Y.; Liu, X. M.; Qian, Y. T. *J. Cryst. Growth* **2003**, *259*, 208−214.

CG049640U